Signal Processing for Aeroacoustic Sensor Networks

Richard J. Kozick* and Brian M. Sadler†

*Bucknell University
Dept. of Electrical Engineering, Lewisburg, PA 17837, USA
Tel: 570-577-1129, Fax: 570-577-1822, e-mail: kozick@bucknell.edu

†Army Research Laboratory
AMSRL-CI-CN, 2800 Powder Mill Road, Adelphi, MD 20783, USA
Tel: 301-394-1239, Fax: 301-394-1197, e-mail: bsadler@arl.army.mil

Abstract

Will we have an abstract? Perhaps a summary of the chapter before the Introduction?

Chapter for *Frontiers in Distributed Sensor Networks*, CRC Press

DRAFT of July 7, 2003

Contents

1 Introduction

Things to bring out in the introduction:

- Include historical discussion. The early ARL work is described in [1], and this TR also lays out many of the fundamental issues. This report is important primarily as it documents ARL and contractor experiments dating to 1992 and 1993, so a good one for us to cite. It is fully releasable and is generally available to anyone via the DTIC system.

- Contrast with conventional array processing literature: Note the propagation issues, and what to do about them. Cite papers by Gershman, Besson, Stoica, Swami/Ghogo, ...

- (Ultra-)wideband signals: frequencies of interest from 30 Hz to 250 Hz. Below 30 Hz (infrasonics): large wavelength and high wind noise. Above 250 Hz: rapid attenuation, so limited range. Sources often emit sounds that are sums-of-harmonics, due to rotating machinery in ground vehicle/aircraft engines, and also due to "tread slap" from tracked vehicles in motion. Perhaps note that seismic sensors are often used simultaneously with microphones? Citations for seismic?

- The wavelength is large relative to the array apertures: At 30 Hz, λ = (330 m/s)/(30 Hz) = 11 m, and at 200 Hz, λ = (330 m/s)/(200 Hz) = 1.65 m. Therefore the wavelengths of interest are from 1 m to 10 m. Microphone arrays typically used in practice have apertures from several meters [1] to less than one meter, e.g., [2].

- Sources may be either far-field or near-field with respect to individual array apertures, and they are almost always near-field with respect to multiple arrays. Ground vehicles and aircraft are loud and can be detected at ranges of 100's or 1,000's of meters.

- Sensor networking and signal processing issues:

  Nodes are connected by wireless communication links, and each node can perform local signal processing. The communication links have limited bandwidth. The low-frequency signals allow low sampling rates and enable sophisticated signal processing. Therefore an important design question is how to perform distributed processing in order to reduce communication

bandwidth while minimizing the degradation in detection, estimation, and classification performance.

- Propagation characteristics for sound in air [3, 4, 5, 6, 7, 8, 9, 10, 11]:
  - Nonhomogeneous, turbulent atmosphere causes random fluctuations in the measured signals, with variations on time scales from 1 to 10's of seconds.
  - This "scattering" of the sound causes loss in the spatial coherence of the signals measured at pairs of sensors, as well as fluctuations in the signal energy at a single sensor. The scattering may be "weak" or "strong," which are analogous to Rician and Rayleigh fading in the radio propagation literature.
- Sources in motion and the presence of multiple sources are typical in the battlefield applications, and these present challenges that must be addressed.

  If very many individual sources are present in clusters, then perhaps best to use nonparametric methods to detect and track the clusters?
- Other issues: Aspect-angle dependence of source signal, Doppler for moving sources, multimode sensing and fusion (e.g., seismic and acoustic sensors).

2 Models for Source Signals and Propagation

**** Add overview paragraph for this section . . . ****

2.1 Models for source signals

Ground vehicles such as tanks and trucks often emit signals that have harmonic structure. The report [1] describes the mechanisms by which the harmonics are produced in the engine cylinders and the track system in tracked vehicles. Turbine engines are not characterized by harmonic lines, but rather have a broadband, flat spectrum at low frequencies. Helicopter sounds are characterized by harmonic structures caused by the main and tail rotors. However, jet engines in aircraft do not contain harmonic lines, but rather have broadband spectra with some strong spectral lines [1].

Thus the sources of interest in aeroacoustic sensor networks typically have spectra that are either harmonic lines or broadband. The signal processing for detection, localization, and classification

is highly dependent on whether the source spectrum is harmonic or broadband. As we will discuss in Section 3, broadband sources allow time-difference of arrival processing for localization, while harmonic sources allow differential Doppler estimation.

Various approaches have been used to model the source signals, including autoregressive (AR) processes, sums of harmonics, and Gaussian random processes. For example, an AR model is used in [13] for signals with spectral lines as well as a broadband component, and then a combination of maximum likelihood estimation (MLE) and a generalized likelihood ratio test (GLRT) is used to detect the signal with a sensor array. A similar AR model is used in [14], and algorithms are proposed to estimate the angle of arrival (AOA) of the source. In [15], the signal from a helicopter is modeled as a sum of harmonics, and an AR model is used to represent broadband interference. Algorithms are proposed for differential Doppler estimation using the sum of harmonics model and for separation of the helicopter signal and interference. In [16], FFT-based methods are investigated to detect signals with harmonic spectra. We have used Gaussian random processes to model both harmonic and broadband sources in [17].

Source signals often have time-varying characteristics due to changes in engine load during acceleration or braking, and due to changing aspect angle of the source. For example, many ground vehicles sound different when the exhaust is facing toward the sensor array than when the exhaust faces away from the array. Modeling these time variations is nontrivial, so the common approach is to assume that the observation interval is short enough so that the source signal characteristics are constant.

2.2 Models for measured sensor signals

In this section, we present a model for the signals received by the sensors in a microphone array. We begin in Section 2.2.1 with the simplest case in which a single nonmoving source emits a sinusoidal waveform, and the atmosphere induces no scattering. Then in Section 2.2.2, we extend the model to include the effects of scattering, and in Section 2.2.3, approximate models for the scattering as a function of source range, frequency, and atmospheric conditions are presented. The model is extended to multiple sources and multiple frequencies (wideband) in Section 2.2.4.

The sinusoidal source signal that is measured at a reference distance of 1 m from the source is

$$s_{\text{ref}}(t) = \sqrt{S_{\text{ref}}}\cos(2\pi f_o t + \chi), \tag{1}$$

where the frequency of the tone is $f_o = \omega_o/(2\pi)$ Hz, the period is T_o sec, the phase is χ, and the amplitude is $\sqrt{S_{\rm ref}}$. The sound waves propagate with wavelength $\lambda = c/f_o$, where c is the speed of sound. The wavenumber is $k = 2\pi/\lambda = \omega_o/c$. We will represent sinusoidal and narrowband signals by their complex envelope, which may be defined in the two ways in (2):

$$\widetilde{s}_{\rm ref}(t) = s_{\rm ref}^{(\rm I)}(t) + j\, s_{\rm ref}^{(\rm Q)}(t) = \left[s_{\rm ref}(t) + j\,\mathcal{H}\left\{s_{\rm ref}(t)\right\}\right] \exp\left(-j2\pi f_o t\right) \tag{2}$$

$$= \sqrt{S_{\rm ref}}\, \exp\left(j\chi\right). \tag{3}$$

We will represent the complex envelope of a quantity with $\widetilde{(\cdot)}$, the in-phase component with $(\cdot)^{(\rm I)}$, the quadrature component with $(\cdot)^{(\rm Q)}$, and the Hilbert transform with $\mathcal{H}\{\cdot\}$. The in-phase (I) and quadrature (Q) components of a signal are obtained by the processing in Figure 2. The FFT is often used to approximate the processing in Figure 2 for a finite block of data, where the real and imaginary parts of the FFT coefficient at frequency f_o are proportional to the I and Q components, respectively. The complex envelope of the sinusoid in (1) is given by (3), which is not time-varying, so the average power is $|\widetilde{s}_{\rm ref}(t)|^2 = S_{\rm ref}$.

It is easy to see for the sinusoidal signal (1) that shifting $s_{\rm ref}(t)$ in time causes a phase shift in the corresponding complex envelope, i.e., $\widetilde{s_{\rm ref}(t-\tau_o)} = \exp(-j2\pi f_o\tau_o)\,\widetilde{s}_{\rm ref}(t)$. A similar property is true for *narrowband* signals whose frequency spectrum is confined to a bandwidth B Hz around a center frequency f_o Hz, where $B \ll f_o$. For a narrowband signal $z(t)$ with complex envelope $\widetilde{z}(t)$, a shift in time is well-approximated by a phase shift in the corresponding complex envelope,

$$\widetilde{z(t-\tau_o)} \approx \exp(-j2\pi f_o\tau_o)\,\widetilde{z}(t) \quad \text{(narrowband approximation)}. \tag{4}$$

Equation (4) is nothing more than the well-known Fourier transform relationship between shifts in time and phase shifts that are linearly proportional to frequency. The approximation is accurate when the frequency band is narrow enough so that the linearly increasing phase shift is close to $\exp(-j2\pi f_o\tau_o)$ over the band.

The source and array geometry is illustrated in Figure 1. The source is located at coordinates (x_s, y_s) in the (x, y) plane. The array contains N sensors, with sensor n located at $(x_o + \Delta x_n, y_o + \Delta y_n)$, where (x_o, y_o) is the center of the array and $(\Delta x_n, \Delta y_n)$ is the relative sensor location. The propagation time from the source to the array center is

$$\tau_o = \frac{d_o}{c} = \frac{1}{c}\left[(x_s - x_o)^2 + (y_s - y_o)^2\right]^{1/2}, \tag{5}$$

**** NEED TO ADD PICTURE ****

Figure 1: Geometry of source and sensor locations.

where d_o is the distance from the source to the array center. The propagation time from the source to sensor n is

$$\tau_n = \frac{d_n}{c} = \frac{1}{c}\left[(x_s - x_o - \Delta x_n)^2 + (y_s - y_o - \Delta y_n)^2\right]^{1/2}. \tag{6}$$

Let us denote the array diameter by $L = \max\{\rho_{mn}\}$, where ρ_{mn} is the separation between sensors m and n, as shown in Figure 1. The source is in the *far-field* of the array when the source distance satisfies $d_o \gg L^2/\lambda$, in which case (6) may be approximated with the first term in the Taylor series $(1+u)^{1/2} \approx 1 + u/2$. Then $\tau_n \approx \tau_o + \tau_{o,n}$ with error that is much smaller than the source period, T_o, where

$$\tau_{o,n} = -\frac{1}{c}\left[\frac{x_s - x_o}{d_o}\Delta x_n + \frac{y_s - y_o}{d_o}\Delta y_n\right] = -\frac{1}{c}\left[(\cos\phi)\Delta x_n + (\sin\phi)\Delta y_n\right]. \tag{7}$$

The angle ϕ is the azimuth bearing, or angle of arrival (AOA), as shown in Figure 1. In the far-field, the spherical wavefront is approximated as a plane wave over the array aperture, so the bearing ϕ contains the available information about the source location. For array diameters $L < 2$ m and tone frequencies $f_o < 200$ Hz so that $\lambda > 1.5$ m, the quantity $L^2/\lambda < 2.7$ m. Thus the far-field is valid for source distances on the order of 10's of meters. For smaller source distances and/or larger array apertures, the curvature of the wavefront over the array aperture must be included in τ_n according to (6). We develop the model for the far-field case in this section. However, the extension to the near-field is easily accomplished by redefining the array response vector ($\mathbf{a}$ in (20)) to include the wavefront curvature with $a_n = \exp(-j2\pi f_o \tau_n)$.

Four phenomena contribute to modify the reference signal in (3) to produce the signals that impinge on the sensor array.

1. Propagation delay from source to sensors, given by τ_n in (6), or the far-field approximation $\tau_n \approx \tau_o + \tau_{o,n}$ with (5) and (7).

2. Random fluctuations in the amplitude and phase of the signals caused by "scattering" in the nonhomogeneous, turbulent atmosphere.

3. Additive noise at the sensors caused by thermal noise, wind noise, and directional interference.

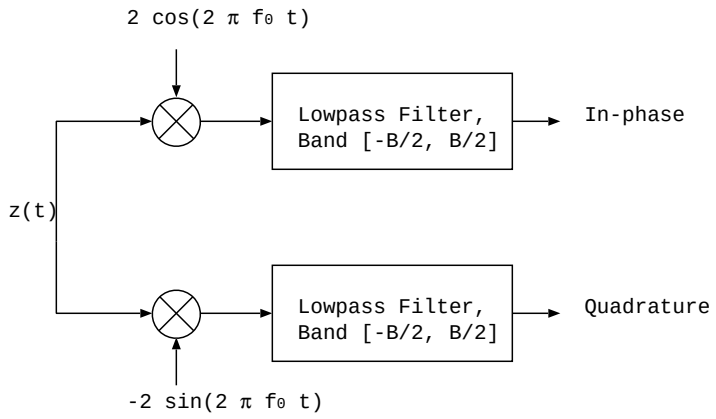

Figure 2: Processing to obtain in-phase and quadrature components, $z^{(\mathrm{I})}(t)$ and $z^{(\mathrm{Q})}(t)$.

4. Transmission loss caused by spherical spreading of the wavefronts, refraction, and ground interactions.

The dominant effect is scattering caused by turbulence, which causes random fluctuations in the complex signals at the sensors. Scattering causes fluctuations in the signal energy at a single sensor and loss in the spatial coherence of signals measured at pairs of sensors. Scattering models are presented in Sections 2.2.2 and 2.2.3. Thermal noise at the sensors is typically independent from sensor to sensor, while wind noise and interference from an undesired source produce additive noise that is (spatially) correlated from sensor to sensor. The transmission loss is difficult to model analytically. A software packaged called the Acoustic Battlefield Aid (ABFA) [3, 4] includes routines to numerically evaluate the transmission loss with a parabolic solution to the wave equation that accounts for spherical spreading, sound refraction by wind and temperature gradients, diffraction, ground interactions, and shadowing behind terrain features such as hills and buildings. The net effect of the transmission loss is that the average power of the source signal impinging on each sensor in the array is S, which is less than the reference power S_{ref} at range 1 m from the source. We do not attempt to model the transformation from S_{ref} to S due to the analytical intractability. Instead, we model S as a deterministic parameter, which is reasonable because S is typically much larger than the average noise power, so the *average* signal to noise ratio (SNR) is large. However, we do model the temporal fluctuations in the signal power caused by scattering, and these random fluctuations have a much more significant impact on signal processing performance than the transmission loss from S_{ref} to S.

The models that we present in this section were developed by Wilson and others in [3, 4, 5, 6, 7, 8, 9, 10, 11]. We refer the reader to these references for details about the physical modeling and for references to the primary source material. The following assumptions and simplifications are implicit in the models. Line-of-sight propagation is assumed (with no multipath), so the models are appropriate for open fields. The additive noise is modeled as independent from sensor to sensor, which ignores the spatial correlation of wind noise that may extend over several meters [18], as well as the effects of interference from an undesired noise source in a particular direction. It is straightforward to extend the models to include spatially-correlated additive noise, but the signal processing may be considerably more complicated in this case (see, e.g., [19]). The random fluctuations caused by scattering are modeled as complex, circular, Gaussian random processes. It is shown in [9] with experimental measurements that the Gaussian model is valid in many conditions, but some measured data indicates non-Gaussian scattering characterized by small amplitude variations with large phase variations. Finally, the sensor array is assumed to be planar, and the models assume near-normal incidence of the wavefronts on the array aperture [7].

2.2.1 Model with no scattering

Here we present the model for the signals impinging on the sensor array when there is no scattering. Using the far-field approximation, the noisy measurements at the sensors are

$$z_n(t) = s_n\left(t - \tau_o - \tau_{o,n}\right) \; + \; w_n(t), \quad n = 1, \ldots, N. \tag{8}$$

In the absence of scattering, the signal components are pure sinusoids,

$$s_n(t) = \sqrt{S}\,\cos\left(2\pi f_o t + \chi\right). \tag{9}$$

The $w_n(t)$ are additive, white, Gaussian noise (AWGN) processes that are real-valued, continuous-time, zero-mean, jointly wide-sense stationary, and mutually uncorrelated at distinct sensors with power spectral density (PSD) $(\mathcal{N}_o/2)$ W/Hz. That is, the noise correlation properties are

$$E\{w_n(t)\} \;\; = \;\; 0, \quad -\infty < t < \infty, \; n = 1, \ldots, N \tag{10}$$

$$r_{w,mn}(\xi) = E\{w_m(t+\xi)w_n(t)\} \;\; = \;\; r_w(\xi)\,\delta_{mn}, \tag{11}$$

where $E\{\cdot\}$ denotes expectation and $r_w(\xi) = (\mathcal{N}_o/2)\,\delta(\xi)$ is the noise autocorrelation function that is common at all sensors. The Dirac delta function is $\delta(\cdot)$, and the Kronecker delta function is

$\delta_{mn} = 1$ if $m = n$ and 0 otherwise. As noted above, modeling the noise as spatially white may be inaccurate if wind noise or interfering sources are present in the environment. The noise PSD is

$$G_w(f) = \mathcal{F}\{r_w(\xi)\} = \frac{\mathcal{N}_o}{2}, \tag{12}$$

where $\mathcal{F}\{\cdot\}$ denotes Fourier transform. With no scattering, the complex envelope of $z_n(t)$ in (8) and (9) is, using (4),

$$\begin{aligned} \widetilde{z}_n(t) &= \exp\left[-j\ (\omega_o \tau_o + \omega_o \tau_{o,n})\right]\ \widetilde{s}_n(t)\ +\ \widetilde{w}_n(t) \\ &= \sqrt{S}\ \exp\left[j\ (\chi - \omega_o \tau_o)\right]\ \exp\left[-j\,\omega_o \tau_{o,n}\right]\ +\ \widetilde{w}_n(t), \end{aligned} \tag{13}$$

where the complex envelope of the source component is

$$\widetilde{s}_n(t) = \sqrt{S}\, e^{j\chi}, \quad n = 1, \ldots, N \quad \text{(no scattering)}. \tag{14}$$

We assume that the complex envelope is lowpass filtered with bandwidth from $[-B/2, B/2]$ Hz, e.g., as in Figure 2. Assuming that the lowpass filter is ideal, the complex envelope of the noise, $\widetilde{w}_n(t)$, has PSD and correlation

$$G_{\tilde{w}}(f) = (2\mathcal{N}_o)\,\mathrm{rect}\left(\frac{f}{B}\right) \tag{15}$$

$$r_{\tilde{w}}(\xi) = E\{\widetilde{w}_n(t+\xi)\widetilde{w}_n(t)^*\} = \mathcal{F}^{-1}\left\{G_{\tilde{w}}(f)\right\} = (2\mathcal{N}_o B)\,\mathrm{sinc}\,(B\xi) \tag{16}$$

$$r_{\tilde{w},mn}(\xi) = E\{\widetilde{w}_m(t+\xi)\widetilde{w}_n(t)^*\} = r_{\tilde{w}}(\xi)\,\delta_{mn}, \tag{17}$$

where $(\cdot)^*$ denotes complex conjugate, $\mathrm{rect}(u) = 1$ for $-1/2 < u < 1/2$ and 0 otherwise, and $\mathrm{sinc}(u) = \sin(\pi u)/(\pi u)$. Note that the noise samples are uncorrelated (and independent since Gaussian) at sample times spaced by $1/B$ sec. In practice, the noise PSD $G_{\tilde{w}}(f)$ is neither flat nor perfectly band-limited as in (15). However, the lowpass filtering to bandwidth B Hz implies that the noise samples have decreasing correlation for time spacing greater than $1/B$ sec.

Let us define the vectors

$$\widetilde{\mathbf{z}}(t) = \begin{bmatrix} \widetilde{z}_1(t) \\ \vdots \\ \widetilde{z}_N(t) \end{bmatrix}, \quad \widetilde{\mathbf{s}}(t) = \begin{bmatrix} \widetilde{s}_1(t) \\ \vdots \\ \widetilde{s}_N(t) \end{bmatrix}, \quad \widetilde{\mathbf{w}}(t) = \begin{bmatrix} \widetilde{w}_1(t) \\ \vdots \\ \widetilde{w}_N(t) \end{bmatrix}. \tag{18}$$

Then using (13) with (7),

$$\widetilde{\mathbf{z}}(t) = \sqrt{S}\ \exp\left[j\ (\chi - \omega_o \tau_o)\right]\ \mathbf{a}\ +\ \widetilde{\mathbf{w}}(t) = \sqrt{S}\, e^{j\theta}\, \mathbf{a}\ +\ \widetilde{\mathbf{w}}(t), \tag{19}$$

where $\mathbf{a}$ is the array steering vector (or array manifold)

$$\mathbf{a} = \begin{bmatrix} \exp\left[j\,k\,\left((\cos\phi)\Delta x_1 + (\sin\phi)\Delta y_1\right)\right] \\ \vdots \\ \exp\left[j\,k\,\left((\cos\phi)\Delta x_N + (\sin\phi)\Delta y_N\right)\right] \end{bmatrix} \tag{20}$$

with $k = \omega_o/c$. Note that the steering vector, $\mathbf{a}$, depends on the frequency ω_o, the sensor locations $(\Delta x_n, \Delta y_n)$, and the source bearing ϕ. The common phase factor at all of the sensors, $\exp\left[j\ (\chi - \omega_o\tau_o)\right] = \exp\left[j\ (\chi - kd_o)\right]$, depends on the phase of the signal emitted by the source (χ) and the propagation distance to the center of the array (kd_o). We simplify the notation and define

$$\theta \stackrel{\triangle}{=} \chi - kd_o, \tag{21}$$

which is a deterministic parameter.

In preparation for the introduction of scattering into the model, let us write expressions for the first- and second-order moments of the vectors $\widetilde{\mathbf{s}}(t)$ and $\widetilde{\mathbf{z}}(t)$. Let $\mathbf{1}$ be an $N \times 1$ vector of 1's, $\mathbf{R}_{\tilde{\mathbf{z}}}(\xi) = E\{\widetilde{\mathbf{z}}(t+\xi)\,\widetilde{\mathbf{z}}(t)^H\}$ be the $N \times N$ cross-correlation function matrix with (m,n) element $r_{\tilde{z},mn}(\xi) = E\{\widetilde{z}_m(t+\xi)\widetilde{z}_n(t)^*\}$, and $\mathbf{G}_{\tilde{\mathbf{z}}}(f) = \mathcal{F}\left\{\mathbf{R}_{\tilde{\mathbf{z}}}(\xi)\right\}$ be the cross-spectral density (CSD) matrix, then

$$E\{\widetilde{\mathbf{s}}(t)\} = \sqrt{S}\,e^{j\chi}\,\mathbf{1} \qquad E\{\widetilde{\mathbf{z}}(t)\} = \sqrt{S}\,e^{j\theta}\,\mathbf{a} \tag{22}$$

$$\mathbf{R}_{\tilde{\mathbf{s}}}(\xi) = S\,\mathbf{1}\mathbf{1}^T \qquad \mathbf{R}_{\tilde{\mathbf{z}}}(\xi) = S\,\mathbf{a}\mathbf{a}^H\ +\ r_{\tilde{w}}(\xi)\,\mathbf{I} \tag{23}$$

$$\mathbf{G}_{\tilde{\mathbf{s}}}(f) = S\,\mathbf{1}\mathbf{1}^T\,\delta(f) \qquad \mathbf{G}_{\tilde{\mathbf{z}}}(f) = S\,\mathbf{a}\mathbf{a}^H\,\delta(f)\ +\ G_{\tilde{w}}(f)\,\mathbf{I} \tag{24}$$

$$E\{\widetilde{\mathbf{s}}(t)\widetilde{\mathbf{s}}(t)^H\} = \mathbf{R}_{\tilde{\mathbf{s}}}(0) = S\,\mathbf{1}\mathbf{1}^T \qquad E\{\widetilde{\mathbf{z}}(t)\widetilde{\mathbf{z}}(t)^H\} = \mathbf{R}_{\tilde{\mathbf{z}}}(0) = S\,\mathbf{a}\mathbf{a}^H\ +\ \sigma^2_{\tilde{w}}\,\mathbf{I}, \tag{25}$$

where $(\cdot)^T$ denotes transpose, $(\cdot)^H$ denotes complex conjugate transpose, $\mathbf{I}$ is the $N \times N$ identity matrix, and $\sigma^2_{\tilde{w}}$ is the variance of the noise samples,

$$\sigma^2_{\tilde{w}} = E\left\{\left|\widetilde{\mathbf{w}}(t)\right|^2\right\} = r_{\tilde{w}}(0) = 2\mathcal{N}_o B. \tag{26}$$

Note from (24) that the PSD at each sensor contains a spectral line since the source signal is sinusoidal. Note from (25) that at each sensor, the average power of the signal component is S, so the signal to noise ratio (SNR) at each sensor is

$$\text{SNR} = \frac{S}{\sigma^2_{\tilde{w}}} = \frac{S}{2\mathcal{N}_o B}. \tag{27}$$

The complex envelope vector $\widetilde{\mathbf{z}}(t)$ is typically sampled at a rate $f_s = B$ samples/sec, so the samples are spaced by $T_s = 1/f_s = 1/B$ sec,

$$\widetilde{\mathbf{z}}(iT_s) = \sqrt{S}\, e^{j\theta}\, \mathbf{a} \;+\; \widetilde{\mathbf{w}}(iT_s), \quad i = 0, \ldots, T-1. \tag{28}$$

According to (17), the noise samples are spatially independent as well as temporally independent, since $r_{\tilde{w}}(iT_s) = r_{\tilde{w}}(i/B) = 0$. Thus the vectors $\widetilde{\mathbf{z}}(0), \widetilde{\mathbf{z}}(T_s), \ldots, \widetilde{\mathbf{z}}((T-1)T_s)$ in (28) are independent and identically distributed (iid) with complex normal distribution, which we denote by $\widetilde{\mathbf{z}}(iT_s) \sim \mathrm{CN}\,(\mathbf{m}_{\tilde{\mathbf{z}}}, \mathbf{C}_{\tilde{\mathbf{z}}})$, with mean and covariance matrix

$$\mathbf{m}_{\tilde{\mathbf{z}}} = \sqrt{S}\, e^{j\theta}\, \mathbf{a} \;\text{ and }\; \mathbf{C}_{\tilde{\mathbf{z}}} = \sigma_{\tilde{w}}^2\, \mathbf{I} \quad \text{(no scattering)}. \tag{29}$$

The joint probability density function for $\mathrm{CN}\,(\mathbf{m}_{\tilde{\mathbf{z}}}, \mathbf{C}_{\tilde{\mathbf{z}}})$ is given by [35]

$$f\,(\widetilde{\mathbf{z}}) = \frac{1}{\pi^N \det\,(\mathbf{C}_{\tilde{\mathbf{z}}})} \exp\left[-\,(\widetilde{\mathbf{z}} - \mathbf{m}_{\tilde{\mathbf{z}}})^H\; \mathbf{C}_{\tilde{\mathbf{z}}}^{-1}\; (\widetilde{\mathbf{z}} - \mathbf{m}_{\tilde{\mathbf{z}}}) \right], \tag{30}$$

where "det" denotes determinant. In the absence of scattering, the information about the source location (bearing) is contained in the mean of the sensor observations. If the T time samples in (28) are coherently averaged, then the resulting SNR per sensor is T times that in (27), so $\mathrm{SNR}' = T \cdot (S/\sigma_{\tilde{w}}^2) = T \cdot [S/(2\mathcal{N}_o/T_s)] = \mathcal{T} \cdot S/(2\mathcal{N}_o)$, where $\mathcal{T} = T \cdot T_s$ is the total observation time, in seconds.

2.2.2 Model with scattering

Next, we include the effects of scattering by the atmosphere in the model for the signals measured at the sensors in the array. Wave propagation through the nonhomogeneous, turbulent atmosphere causes random fluctuations in the measured signals, with variations on time scales from 1 to 10's of seconds. As noted previously, the model that we present was developed by Wilson and others [3, 4, 5, 6, 7, 8, 9, 10, 11]. The model in Section 2.2.1 for propagation without scattering assumed line of sight propagation (no multipath), and the scattering model maintains this assumption.

The scattering modifies the complex envelope of the signals at the array by spreading a portion of the power from the (deterministic) mean component into a zero-mean random process with a PSD centered at 0 Hz. We assume that the bandwidth of the scattered signal, which we denote by B, is much smaller than the tone frequency, f_o. The "saturation" parameter [3, 4, 5, 6, 7, 8], denoted by $\Omega \in [0, 1]$, defines the fraction of average signal power that is scattered from the mean

into the random component. The scattering may be "weak" ($\Omega \approx 0$) or "strong" ($\Omega \approx 1$), which are analogous to Rician and Rayleigh fading in the radio propagation literature. The modification of (8), (9), (13), and (14) to include scattering is as follows, where $\widetilde{z}_n(t)$ is the signal measured at sensor n:

$$\widetilde{z}_n(t) = \exp\left[-j\ (\omega_o \tau_o + \omega_o \tau_{o,n})\right]\ \widetilde{s}_n(t)\ +\ \widetilde{w}_n(t) \tag{31}$$

$$\widetilde{s}_n(t) = \sqrt{(1-\Omega)S}\, e^{j\chi}\ +\ \widetilde{v}_n(t)\, e^{j\chi},\ \ n = 1, \ldots, N \text{ (with scattering)}. \tag{32}$$

In order to satisfy conservation of energy with $E\{|\widetilde{s}_n(t)|^2\} = S$, the average power of the scattered component must be $E\{|\widetilde{v}_n(t)|^2\} = \Omega\, S$. The value of the saturation Ω and the correlation properties of the vector of scattered processes, $\widetilde{\mathbf{v}}(t) = [\widetilde{v}_1(t), \ldots, \widetilde{v}_N(t)]^T$, depend on the source distance (d_o) and the meteorological conditions. The vector of scattered processes $\widetilde{\mathbf{v}}(t)$ and the additive noise vector $\widetilde{\mathbf{w}}(t)$ contain zero-mean, jointly wide-sense stationary, complex, circular Gaussian random processes. The scattered processes and the noise are modeled as independent, $E\{\widetilde{\mathbf{v}}(t+\xi)\widetilde{\mathbf{w}}(t)^H\} = \mathbf{0}$. The noise is described by (15)-(17), while the saturation Ω and statistics of $\widetilde{\mathbf{v}}(t)$ are determined by the "extinction coefficients" of the first and second moments of $\widetilde{\mathbf{s}}(t)$. Approximate models for the extinction coefficients are available from physical modeling of the turbulence in the atmosphere [cite Wilson]. In the remainder of this section, we define the extinction coefficients and relate them to Ω and the statistics of $\widetilde{\mathbf{v}}(t)$. Then in Section 2.2.3, we provide approximate analytical expressions for the extinction coefficients under several meteorological conditions, thereby providing models for the sensor array data that includes the turbulent scattering by the atmosphere.

We denote the extinction coefficients for the first and second moments of $\widetilde{\mathbf{s}}(t)$ by μ and $\nu(\rho_{mn})$, respectively, where ρ_{mn} is the distance between sensors m and n (see Figure 1). The extinction coefficients are defined as follows.

$$E\{\widetilde{s}_n(t)\} = \sqrt{(1-\Omega)S}\, e^{j\chi} \qquad \stackrel{\triangle}{=} \sqrt{S}\, e^{j\chi}\, e^{-\mu d_o} \tag{33}$$

$$r_{\tilde{s},mn}(0) = E\{\widetilde{s}_m(t)\widetilde{s}_n(t)^*\} = (1-\Omega)S\ +\ r_{\tilde{v},mn}(0) \qquad \stackrel{\triangle}{=} S\, e^{-\nu(\rho_{mn})d_o} \tag{34}$$

where

$$r_{\tilde{s},mn}(\xi) = E\{\widetilde{s}_m(t+\xi)\widetilde{s}_n(t)^*\} = (1-\Omega)S\ +\ r_{\tilde{v},mn}(\xi). \tag{35}$$

The right sides of (33) and (34) are the first and second moments *without* scattering, from (22) and (23), respectively, multiplied by a factor that decays exponentially with increasing distance d_o

from the source. From (33), we obtain

$$\sqrt{(1-\Omega)} = e^{-\mu d_o} \text{ and } \Omega = 1 - e^{-2\mu d_o}. \tag{36}$$

Also, by conservation of energy with $m = n$ in (34), adding the average powers in the unscattered and scattered components of $\widetilde{s}_n(t)$ must equal S, so

$$r_{\tilde{s}}(0) = E\{|\widetilde{s}_n(t)|\} = e^{-2\mu d_o} S \; + \; r_{\tilde{v}}(0) = S \tag{37}$$

$$\Longrightarrow r_{\tilde{v}}(0) = E\{|\widetilde{v}_n(t)|\} = \int_{-\infty}^{\infty} G_{\tilde{v}}(f)\, df = \left(1 - e^{-2\mu d_o}\right) S = \Omega\, S, \tag{38}$$

where $r_{\tilde{v}}(\xi) = E\{\widetilde{v}_n(t+\xi)\widetilde{v}_n(t)^*\}$ is the autocorrelation function (which is the same for all n) and $G_{\tilde{v}}(f)$ is the corresponding PSD. Therefore for source distances $d_o \ll 1/(2\mu)$, the saturation $\Omega \approx 0$ and most of the energy from the source arrives at the sensor in the unscattered (deterministic mean) component of $\widetilde{s}_n(t)$. For source distances $d_o \gg 1/(2\mu)$, the saturation $\Omega \approx 1$ and most of the energy arrives in the scattered (random) component.

Next, we use (34) to relate the correlation of the scattered signals at sensors m and n, $r_{\tilde{v},mn}(\xi)$, to the second moment extinction coefficient, $\nu(\rho_{mn})$. Since the autocorrelation of $\widetilde{v}_n(t)$ is identical at each sensor n and equal to $r_{\tilde{v}}(\xi)$, and assuming that the PSD $G_{\tilde{v}}(f)$ occupies a narrow bandwidth centered at 0 Hz, the cross-correlation and cross-spectral density satisfy

$$r_{\tilde{v},mn}(\xi) = \gamma_{mn}\, r_{\tilde{v}}(\xi) \text{ and } G_{\tilde{v},mn}(f) = \mathcal{F}\{r_{\tilde{v},mn}(\xi)\} = \gamma_{mn} G_{\tilde{v}}(f), \tag{39}$$

where $|\gamma_{mn}| \leq 1$ is a measure of the coherence between $\widetilde{v}_m(t)$ and $\widetilde{v}_n(t)$. The definition of γ_{mn} as a *constant* includes an approximation that the coherence does not vary with frequency, which is reasonable since the bandwidth of $G_{\tilde{v}}(f)$ is narrow. For sensor arrays near ground level, the autocorrelation function of the scattered signal, $r_{\tilde{v}}(\xi)$, remains correlated over time scales from approximately 1 to 10 seconds [3, 4]. Therefore the bandwidth of $G_{\tilde{v}}(f)$ is on the order of 0.1 to 1 Hz. The bandwidth B in the lowpass filters for the complex amplitude in Figure 2 should be chosen to be equal to the bandwidth of $G_{\tilde{v}}(f)$. We assume that γ_{mn} in (39) is real-valued and non-negative, which implies that phase fluctuations at sensor pairs are not biased toward positive or negative values. Then using (39) with (38) and (36) in (34) yields the following relation between γ_{mn} and μ, ν:

$$\gamma_{mn} = \frac{e^{-\nu(\rho_{mn})d_o} - e^{-2\mu d_o}}{1 - e^{-2\mu d_o}}, \quad m, n = 1, \ldots, N. \tag{40}$$

We define $\mathbf{\Gamma}$ as the $N \times N$ matrix with elements γ_{mn}. The second moment extinction coefficient $\nu(\rho_{mn})$ is a monotonically increasing function, with $\nu(0) = 0$ and $\nu(\infty) = 2\mu$, so $\gamma_{mn} \in [0, 1]$.

Combining (31) and (32) into vectors, and using (36) yields

$$\widetilde{\mathbf{z}}(t) = \sqrt{S}\, e^{j\theta}\, e^{-\mu d_o}\, \mathbf{a} \;+\; e^{j\theta}\, \mathbf{a}\, \widetilde{\mathbf{v}}(t) \;+\; \widetilde{\mathbf{w}}(t), \tag{41}$$

where θ is defined in (21) and $\mathbf{a}$ is the array steering vector in (20). We define the matrix $\mathbf{B}$ with elements

$$B_{mn} = \exp\left[-\nu(\rho_{mn}) d_o\right], \tag{42}$$

and then we can extend the second-order moments in (22)-(25) to the case with scattering as

$$E\{\widetilde{\mathbf{z}}(t)\} = e^{-\mu d_o}\, \sqrt{S}\, e^{j\theta}\, \mathbf{a} \stackrel{\triangle}{=} \mathbf{m}_{\tilde{\mathbf{z}}} \tag{43}$$

$$\mathbf{R}_{\tilde{\mathbf{z}}}(\xi) = e^{-2\mu d_o}\, S\, \mathbf{a}\mathbf{a}^H \;+\; S\, \left[\mathbf{B} \circ \left(\mathbf{a}\mathbf{a}^H\right) - e^{-2\mu d_o}\, \mathbf{a}\mathbf{a}^H\right] \frac{r_{\tilde{v}}(\xi)}{S\left(1 - e^{-2\mu d_o}\right)} \;+\; r_{\tilde{w}}(\xi)\, \mathbf{I} \tag{44}$$

$$\mathbf{G}_{\tilde{\mathbf{z}}}(f) = e^{-2\mu d_o}\, S\, \mathbf{a}\mathbf{a}^H\, \delta(f) + \;S\, \left[\mathbf{B} \circ \left(\mathbf{a}\mathbf{a}^H\right) - e^{-2\mu d_o}\, \mathbf{a}\mathbf{a}^H\right] \frac{G_{\tilde{v}}(f)}{S\left(1 - e^{-2\mu d_o}\right)} \;+\; G_{\tilde{w}}(f)\, \mathbf{I} \tag{45}$$

$$E\{\widetilde{\mathbf{z}}(t)\widetilde{\mathbf{z}}(t)^H\} = \mathbf{R}_{\tilde{\mathbf{z}}}(0) = S\, \mathbf{B} \circ \left(\mathbf{a}\mathbf{a}^H\right) \;+\; \sigma_{\tilde{w}}^2\, \mathbf{I} \stackrel{\triangle}{=} \mathbf{C}_{\tilde{\mathbf{z}}} \;+\; \mathbf{m}_{\tilde{\mathbf{z}}}\, \mathbf{m}_{\tilde{\mathbf{z}}}^H, \tag{46}$$

where $\circ$ denotes element-wise product between matrices. The normalizing quantity $S\left(1 - e^{-2\mu d_o}\right)$ that divides the autocorrelation $r_{\tilde{v}}(\xi)$ and the PSD $G_{\tilde{v}}(f)$ in (44) and (45) is equal to $r_{\tilde{v}}(0) = \int G_{\tilde{v}}(f)\, df$. Therefore the maximum of the normalized autocorrelation is 1, and the area under the normalized PSD is 1. The complex envelope samples $\widetilde{\mathbf{z}}(t)$ have the complex normal distribution $\mathrm{CN}\left(\mathbf{m}_{\tilde{\mathbf{z}}}, \mathbf{C}_{\tilde{\mathbf{z}}}\right)$, which is defined in (30). The mean vector and covariance matrix are given in (43) and (46), but we repeat them below for comparison with (29),

$$\mathbf{m}_{\tilde{\mathbf{z}}} = e^{-\mu d_o}\, \sqrt{S}\, e^{j\theta}\, \mathbf{a} \qquad \text{(with scattering)} \tag{47}$$

$$\mathbf{C}_{\tilde{\mathbf{z}}} = S\, \left[\mathbf{B} \circ \left(\mathbf{a}\mathbf{a}^H\right) - e^{-2\mu d_o}\, \mathbf{a}\mathbf{a}^H\right] \;+\; \sigma_{\tilde{w}}^2\, \mathbf{I} \qquad \text{(with scattering).} \tag{48}$$

Note that the scattering is negligible if $d_o \ll 1/(2\mu)$, in which case $e^{-2\mu d_o} \approx 1$ and $\Omega \approx 0$. Then most of the signal energy is in the mean, with $\mathbf{B} \approx \mathbf{1}\mathbf{1}^T$ and $\gamma_{mn} \approx 1$ in (40), since $\nu(\rho_{mn}) < 2\mu$. For larger values of the source range d_o, more of the signal energy is scattered, and $\mathbf{B}$ may deviate from $\mathbf{1}\mathbf{1}^T$ (and $\gamma_{mn} < 1$ for $m \neq n$) due to coherence losses between the sensors. At full saturation ($\Omega = 1$), $\mathbf{B} = \mathbf{\Gamma}$.

The scattering model in (41) may be formulated as multiplicative noise on the steering vector,

$$\widetilde{\mathbf{z}}(t) = \sqrt{S}\, e^{j\theta}\, \mathbf{a} \circ \left[e^{-\mu d_o}\, \mathbf{1} \;+\; \frac{\widetilde{\mathbf{v}}(t)}{\sqrt{S}} \right] \;+\; \widetilde{\mathbf{w}}(t) \;\triangleq\; \sqrt{S}\, e^{j\theta}\, (\mathbf{a} \circ \widetilde{\mathbf{u}}(t)) \;+\; \widetilde{\mathbf{w}}(t). \tag{49}$$

The multiplicative noise process, $\widetilde{\mathbf{u}}(t)$, is complex normal with $\mathbf{m}_{\widetilde{\mathbf{u}}} = E\{\widetilde{\mathbf{u}}(t)\} = e^{-\mu d_o}\, \mathbf{1}$ and $E\{\widetilde{\mathbf{u}}(t)\, \widetilde{\mathbf{u}}(t)^H\} = \mathbf{B}$, so the covariance matrix is $\mathbf{C}_{\widetilde{\mathbf{u}}} = \mathbf{B} - e^{-2\mu d_o}\, \mathbf{1}\mathbf{1}^T = \Omega\mathbf{\Gamma}$, where $\mathbf{\Gamma}$ has elements γ_{mn} in (40). The mean vector and covariance matrix in (47) and (48) may be represented as $\mathbf{m}_{\widetilde{\mathbf{z}}} = \sqrt{S}\, e^{j\theta}\, (\mathbf{a} \circ \mathbf{m}_{\widetilde{\mathbf{u}}})$ and $\mathbf{C}_{\widetilde{\mathbf{z}}} = S\, \left[\left(\mathbf{a}\mathbf{a}^H \right) \circ \mathbf{C}_{\widetilde{\mathbf{u}}} \right] \;+\; \sigma_{\widetilde{w}}^2\, \mathbf{I}$.

The sampling rate $f_s = 1/T_s$ for the complex envelope is determined by the coherence bandwidth, B, of the scattered process. As discussed in the text below (39), B is on the order of 0.1 to 1 Hz so samples spaced by $T_s \approx 1/B = 1$ to 10 seconds are independent.

2.2.3 Model for extinction coefficients

We present approximate models for the extinction coefficients of the first and second moments, μ and $\nu(\rho)$. The approximate formulas are obtained by fitting linear models to the log-log plots in Figures 4 and 5 of [6]. Both coefficients depend quadratically on the frequency of the tone, although this frequency dependence is not shown explicitly in the notation. For sensor separations, ρ, in the range from 0.1 to 10 m, the second moment coefficient is

$$\nu(\rho) \approx \begin{cases} \left(1.52 \times 10^{-10}\right)\, f^2\, \rho^{1.3}, & \text{mostly cloudy and calm} \\ \left(1.51 \times 10^{-9}\right)\, f^2\, \rho^{1.3}, & \text{mostly sunny and calm} \\ \left(1.58 \times 10^{-9}\right)\, f^2\, \rho^{1.2}, & \text{windy and (sunny or cloudy)} \end{cases}, \tag{50}$$

where f is in Hz, ρ is in m, and ν is in m^{-1}. The value of $\nu(\rho)$ affects the sensor signals according $\exp(-\nu(\rho) d_o)$, where d_o is the distance to the source. Note from (50) that in calm conditions (no wind), the same value of $\exp(-\nu(\rho) d_o)$ is maintained for source distances that are 10 times larger in cloudy conditions than in sunny conditions. The presence of wind nullifies the advantages of cloudy conditions over sunny conditions.

Recall from the discussion after (40) that $\nu(\rho) \to 2\mu$ as the sensor separation ρ gets large. The approximation (50) is valid for ρ between 0.1 and 10 m, and then there is a transition to the asymptotic value of 2μ for ρ between 10 and 1000 m.¡ The asymptotic value is reached for ρ between 100 and 1000 m, which yields the approximation of the first moment coefficient as $\mu = (1/2)\alpha(\infty)$,

$$\mu = \begin{cases} 10^{-7}\, f^2, & \text{cloudy} \\ 3 \times 10^{-7}\, f^2, & \text{sunny} \end{cases}. \tag{51}$$

The wind has negligible effect on the first moment coefficient μ. The value of μ affects the saturation according to $\Omega = 1 - \exp(-2\mu d_o)$ as in (36). For the same value of Ω, the source distance d_o may be about three times larger in cloudy conditions than in sunny conditions. These results from [6] were obtained by incorporating both the inertial-subrange and the energy-subrange (large-scale) of the turbulence spectrum [10]. The calculations in [6] were performed for a propagation path height of 1 m.

Let us evaluate the saturation Ω for some typical scenarios in aeroacoustics. At $f = 100$ Hz with cloudy conditions, the saturation is $\Omega = 1 - \exp(-2 \times 10^{-3} d_o)$. So for $d_o \ll 500$ m, the saturation $\Omega \approx 0$ and the scattering is weak, while for $d_o \gg 500$ m, the saturation $\Omega \approx 1$ and the scattering is strong. At $d_o = 10, 100$, and 1000 m, the saturation is $\Omega \approx 0.02, 0.2$, and 0.86, respectively. Thus the entire range of saturation values from 0 to 1 may be encountered in aeroacoustic applications, which typically have source ranges from meters to kilometers.

Figure 3 illustrates the coherence of the scattered signals, γ_{mn} in (40), as a function of the sensor separation, ρ. The extinction coefficients in (50), (51) are computed at frequency $f = 100$ Hz and source range $d_o = 1,000$ m, with mostly cloudy, calm conditions ($\Omega = 0.86$). Note the coherence is nearly perfect for sensor separations $\rho < 1$ m, but the coherence declines steeply for large separations, with slope -0.0044 m^{-1} at $\rho = 10$ m.

2.2.4 Multiple frequencies and sources

The model in (49) is for a single source that emits a single frequency, $\omega = 2\pi f_o$ rad/s. The complex envelope processing in (2) and Figure 2 is a function of the source frequency. We can extend the model in (49) to the case of K sources that emit tones at L frequencies $\omega_1, \ldots, \omega_L$, as follows:

$$\widetilde{\mathbf{z}}(iT_s;\omega_l) = \sum_{k=1}^{K} \sqrt{S_k(\omega_l)}\, e^{j\theta_{k,l}}\, (\mathbf{a}_k(\omega_l) \circ \widetilde{\mathbf{u}}_k(iT_s;\omega_l)) \;+\; \widetilde{\mathbf{w}}(iT_s;\omega_l), \quad \begin{matrix} i = 1,\ldots,T \\ l = 1,\ldots,L \end{matrix} \tag{52}$$

$$= ([\mathbf{a}_1(\omega_l) \ldots \mathbf{a}_K(\omega_l)] \circ [\widetilde{\mathbf{u}}_1(iT_s;\omega_l) \ldots \widetilde{\mathbf{u}}_K(iT_s;\omega_l)]) \begin{bmatrix} \sqrt{S_1(\omega_l)}\, e^{j\theta_{1,l}} \\ \vdots \\ \sqrt{S_K(\omega_l)}\, e^{j\theta_{K,l}} \end{bmatrix} + \widetilde{\mathbf{w}}(iT_s;\omega_l)$$

$$\triangleq \Big(\mathbf{A}(\omega_l) \circ \widetilde{\mathbf{U}}(iT_s;\omega_l)\Big)\, \widetilde{\mathbf{p}}(\omega_l) \;+\; \widetilde{\mathbf{w}}(iT_s;\omega_l). \tag{53}$$

In (52), $S_k(\omega_l)$ is the average power of source k at frequency ω_l, $\mathbf{a}_k(\omega_l)$ is the steering vector for source k at frequency ω_l as in (20), $\widetilde{\mathbf{u}}_k(iT_s;\omega_l)$ is the scattering of source k at frequency ω_l at

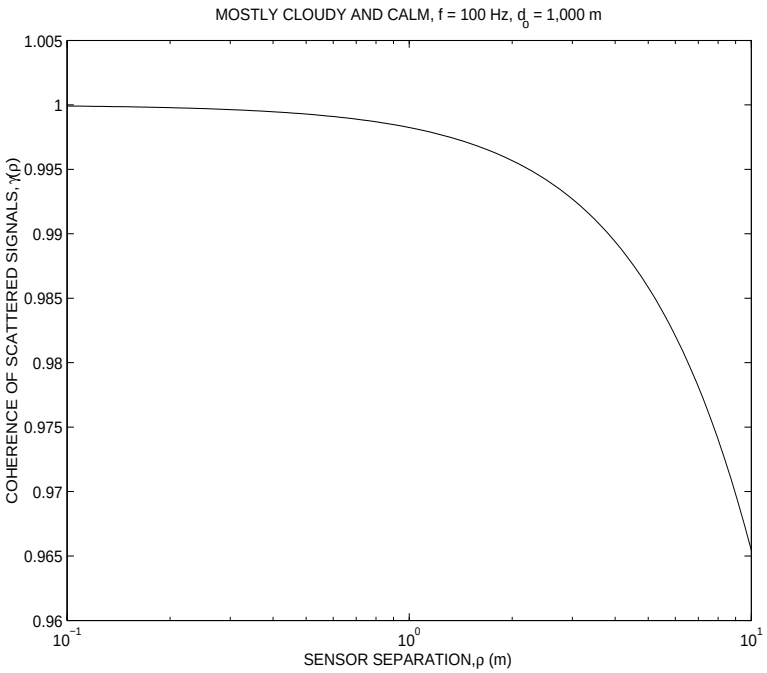

Figure 3: Evaluation of the coherence of the scattered signals measured at sensors with separation ρ using (40) and (50), (51) with $f = 100$ Hz, $d_o = 1,000$ m, $\Omega = 0.86$, and mostly cloudy, calm conditions.

time sample i, and T is the number of time samples. In (53), the steering vector matrices $\mathbf{A}(\omega_l)$, the scattering matrices $\widetilde{\mathbf{U}}(iT_s;\omega_l)$, and the source amplitude vectors $\widetilde{\mathbf{p}}(\omega_l)$ for $l = 1,\ldots,L$ and $i = 1,\ldots,T$, are defined by the context. If the sample spacing T_s is chosen appropriately, then the samples at a given frequency ω_l are independent in time. We will also model the scattered signals at different frequencies as independent. Cross-frequency coherence has been studied theoretically and experimentally, with [9, 20] presenting experimental studies in the atmosphere. However, models for cross-frequency coherence in the atmosphere are at a very preliminary stage. It may be possible to revise the assumption of independent scattering at different frequencies as better models become available.

The covariance matrix at frequency ω_l is, by extending the discussion following (49),

$$\mathbf{C}_{\tilde{\mathbf{z}}}(\omega_l) = \sum_{k=1}^{K} S_k(\omega_l)\,\Omega_k(\omega_l)\,\left[\mathbf{\Gamma}_k(\omega_l) \circ \left(\mathbf{a}_k(\omega_l)\mathbf{a}_k(\omega_l)^H\right)\right] \;+\; \sigma_{\tilde{w}}(\omega_l)^2\,\mathbf{I}, \tag{54}$$

where the scattered signals from different sources are assumed to be independent. If we assume full saturation ($\Omega_k(\omega_l) = 1$) and negligible coherence loss across the array aperture ($\mathbf{\Gamma}_k(\omega_l) = \mathbf{1}\mathbf{1}^T$), then the sensor signals in (52) have zero mean, and the covariance matrix in (54) reduces to the

familiar correlation matrix of the form

$$\begin{aligned}\mathbf{R}_{\widetilde{\mathbf{z}}}(0;\omega_l) &= E\left\{\widetilde{\mathbf{z}}(iT_s;\omega_l)\,\widetilde{\mathbf{z}}(iT_s;\omega_l)^H\right\} \\ &= \mathbf{A}(\omega_l)\,\mathbf{S}(\omega_l)\,\mathbf{A}(\omega_l)^H \;+\; \sigma_{\tilde{w}}(\omega_l)^2\,\mathbf{I} \qquad (\Omega_k(\omega_l)=1 \text{ and no coherence loss}), \end{aligned} \tag{55}$$

where $\mathbf{S}(\omega_l)$ is a diagonal matrix with $S_1(\omega_l),\ldots,S_K(\omega_l)$ along the diagonal.[1]

3 Signal Processing

In this section, we discuss signal processing issues for aeroacoustic sensor networks. The signal processing takes into account the source and propagation models presented in the previous section, as well as minimization of the communication bandwidth between sensor nodes connected by a wireless link. We begin with angle of arrival (AOA) estimation using a single sensor array in Section 3.1. Then we discuss source localization with multiple sensor arrays in Section 3.2, and we briefly describe implications for detection and classification algorithms in Section 3.3.

3.1 Angle of arrival estimation

We discuss narrowband AOA estimation with scattering in Section 3.1.1, and then we discuss wideband AOA estimation without scattering in Section 3.1.2. To our knowledge, the general case of wideband AOA estimation with multiple sources and scattering has not been studied.

3.1.1 Narrowband AOA estimation with scattering

In this section, we review some performance analyses and algorithms that have been investigated for narrowband AOA estimation with scattering. Most of the methods are based on scattering models that are similar to the single-source model in Section 2.2.2 or the multiple-source model in Section 2.2.4 at a single frequency. Many of the references cited below are formulated for radio frequency (RF) channels, so the scattering is caused by multipath propagation and Doppler. However, the models for the sensor data are similar to those presented in Section 2.2.

Wilson [5] analyzed the Cramér-Rao bound (CRB) on AOA estimation for a single source using several models for atmospheric turbulence. Collier and Wilson extended the work [7, 8]

[1] For the fully saturated case with no coherence loss, we can relax the assumption that the scattered signals from different sources are independent by replacing the diagonal matrix $\mathbf{S}(\omega_l)$ in (55) with a positive semidefinite matrix with (m,n) element $\sqrt{S_m(\omega_l)S_n(\omega_l)}\cdot E\{\widetilde{u}_m(iT_s;\omega_l)\widetilde{u}_n(iT_s;\omega_l)^*\}$, where $\widetilde{u}_m(iT_s;\omega_l)$ is the scattered signal for source m.

to include unknown turbulence parameters in the CRB, along with the source AOA. Their CRB analysis provides insight into the combinations of atmospheric conditions, array geometry, and source location that are favorable for accurate AOA estimation. They note that accurate estimation of elevation angle is difficult when the source and sensors are near the ground, so aeroacoustic sensor arrays are most effective for azimuth estimation in these scenarios. Wilson and others have incorporated the CRBs along with several AOA estimation algorithms and terrain models in the ABFA software package [3, 4]. ABFA can be used to simulate scattering in various atmospheric conditions, and Monte Carlo simulations test the performance of AOA estimation algorithms.

Other researchers that have investigated the problem of imperfect spatial coherence in the context of narrowband AOA estimation include [21]–[29] and [19]. Pauraj and Kailath [21] presented a MUSIC algorithm that incorporates nonideal spatial coherence, assuming that the coherence losses are known. Song and Ritcey [22] provided maximum-likelihood (ML) methods for estimating the angles of arrival and the parameters in a coherence model. Gershman et al. [23] provided a procedure to jointly estimate the spatial coherence loss and the angles of arrival. In the series of papers [24]–[27], stochastic and deterministic models were studied for imperfect spatial coherence, and the performance of various AOA estimators was analyzed. Ghogho and Swami [28] presented an algorithm for AOA estimation with multiple sources in the fully-saturated case. Their algorithm exploits the Toeplitz structure of the $\mathbf{B}$ matrix in (42) for a uniform linear array (ULA).

None of the references [21]–[28] handle range of scattering scenarios from weak ($\Omega = 0$) to strong ($\Omega = 1$). Fuks, Goldberg, and Messer [29] treat the case of Rician scattering on RF channels, so this approach does include the entire range from weak to strong scattering. Indeed, the "Rice factor" in the Rician fading model is related to the saturation parameter through $(1 - \Omega)/\Omega$. The main focus in [29] is on CRBs for AOA estimation. The recent paper by Stoica, Agrawal, and Ahgren [19] appears to be the first general study of AOA estimation with non-zero mean signals in the presence of spatially colored noise. The results in [19] are not immediately applicable to the aeroacoustic model in Section 2.2, because [19] is oriented toward wireless communication systems in which the source signals are under control of the designer. However, some results from [19] may be useful for the passive aeroacoustic processing.

**** Perhaps show example from [17] illustrating high coherence over the aperture of an 8 ft diameter array? ****

3.1.2 Wideband AOA estimation without scattering

From Brian's draft of June 10, 2003:

Aeroacoustics is inherently an ultra-wideband array processing problem, e.g., operating in $[50, 250]$ Hz yields a 133% fractional bandwidth centered at 150 Hz. To process under the narrow band array assumptions will require the fractional bandwidth to be on the order of a few percent or less, limiting the bandwidth to perhaps a few Hz in this example. The wide bandwidth significantly complicates the array signal processing, including angle-of-arrival (AOA) estimation, wideband Doppler compensation, beamforming, and blind source separation (which becomes convolutional). Conventional covariance-based narrow band AOA methods break down; the signal subssubpace grows beyond a rank one contribution as the signal bandwidth increases.

A variety of methods are available for wideband AOA estimation, with varying complexity and applicability. Application of these to specific practical problems leads to a complicated task of appropriate procedure choice. We outline some of these methods and various tradeoffs, and describe some experimental results. Basic approaches include: classical delay-and-sum beamformer, incoherent averaging over narrow band spatial spectra, maximum likelihood, coherent signal subspace methods, steered matrix techniques, spatial resampling (array interpolation), and frequency-invariant beamforming. Useful overviews include Boehme [31], and Van Trees [48]. Significant progress in this area has occured in the previous 15 years or so; major earlier efforts include the underwater acoustics area, e.g., see Owsley [38].

Using frequency decomposition at each sensor, we can write (e.g., see [31])

$$X_i(\omega_k) = A(\omega_k)S_i(\omega_k) + N_i(\omega_k), \tag{56}$$

where i indexes the snapshot (time), and ω_k is the kth frequency. The spectral density matrix (SDM) at the frequency ω_k can be defined as

$$R_x(\omega_k) = E[X_i(\omega_k)X_i^H(\omega_k)] = A(\omega_k)R_s(\omega_k)A^H(\omega_k) + R_N(\omega_k). \tag{57}$$

Equation (57) may be interpreted as the covariance matrix of the Fourier-transformed (narrowband) observations (56). The noise is typically assumed to be Gaussian and spatially white, so that $R_N(\omega_k) = \sigma^2(\omega_k)I$. Generalizations to spatially correlated noise are also possible, which may be useful for modeling unknown spatial interference [ref?].

Working with an estimate $\hat{R}_x(\omega_k)$, we may apply covariance-based high resolution AOA estimators (MUSIC, MLE, etc.), although this results in many frequency-dependent angle estimates that must be associated in some way for each source. A simple approach is to sum the resulting narrowband spatial spectra, e.g., see [44]; this is referred to as *noncoherent averaging*. This approach has the advantages of straightforward extension of narrowband methods and relatively low complexity, but can produce artifacts. And, noncoherent averaging requires that the SNRs after channelization be adequate to support the chosen narrow band AOA estimator; in effect the method does not take strong advantage of the wideband nature of the signal. However, loud sum-of-harmonic sources can be processed in this manner with success.

A more general approach was first developed by Wang and Kaveh [49], based on the following additive composition of transformed narrowband SDMs,

$$R_s(\theta_i) = \sum_k T(\theta_i, \omega_k) R_x(\omega_k) T^H(\theta_i, \omega_k), \tag{58}$$

where θ_i is the ith AOA. $R_s(\theta_i)$ is referred to as the *steered covariance matrix* or the *focused wideband covariance matrix*. The transformation matrix $T(\theta_i, \omega_k)$, sometimes called the *focusing matrix*, can be viewed as selecting delays to coincide with delay-sum beamforming, so that the transformation depends on both AOA and frequency. Viewed in another way, the transformation matrix acts to align the signal subspaces, so that the resulting matrix $R_s(\theta_i)$ has a rank one contribution from a wideband source at angle θ_i. Now, narrowband covariance-based methods may be applied to the collection $R_s(\theta_i)$. This approach is generally referred to as the *coherent subspace method* (CSM). CSM has significant advantages: it can handle correlated sources (due to the averaging over frequencies), it averages over the entire source bandwidth, and has good statistical stability. On the other hand, it requires significant complexity, and as originally proposed requires pre-estimation of the AOAs which can lead to biased estimates [45].

A major drawback to CSM is the dependence of T on the the AOA. The most general form requires generation and eigendecomposition of $R_s(\theta_i)$ for each frequency and each look angle; this is clearly undesirable from a computational standpoint.[2] The dependence of T on θ_i can be removed in some cases by incorporating spatial interpolation, thereby greatly reducing the complexity. The

[2] In their original work, Wang and Kaveh relied on pre-estimates of the AOAs to lower the computational burden [49].

basic ideas are established by Krolik and Swingler in [36]; for an overview (including CSM methods) see Krolik [37].

As an example, consider a uniform linear array (ULA) [36, 37], with $d = \lambda_i/2$ spacing. In order to process over another wavelength choice λ_j ($\lambda_j < \lambda_i$), we could spatially interpolate the physical array to a virtual array with the desired spacing ($d_j = \lambda_j/2$). The spatial resampling approach adjusts the spatial sampling interval d as a function of source wavelength λ_j. The result is a simplification of (58) to

$$\tilde{R}(\omega_k) = \sum_k T(\omega_k) R_x(\omega_k) T^H(\omega_k), \tag{59}$$

where the angular dependence is now removed. The resampling acts to align the signal subspace contributions over frequency, so that a single wideband source results in a rank one contribution to $\tilde{R}$. Note that the spatial resampling is implicit in (59). Conventional narrow band AOA estimation methods may now be applied to $\tilde{R}$ and, in contrast to CSM, this operation is conducted once for all angles.

Extensions of [36] from ULAs to arbitrary array geometries can be undertaken, but the dependence on look angle returns, and the resulting complexity is then similar to the CSM approaches. To avoid this, Friedlander and Weiss considered spatial interpolation of an arbitrary physical array to virtual arrays that are uniform and linear [34], thereby returning to a formulation like (59). Doron et al. [33] developed a spatial interpolation method for forming a focused covariance matrix with arbitrary arrays. The formulation relies on a truncated series expansion of plane waves in polar coordinates. The array manifold vector is now separable, allowing focusing matrices that are not a function of angle. The specific case of a *circular* array leads to an FFT-based implementation that is appealing from a low complexity standpoint.

While the spatial resampling methods are clearly desirable from a complexity standpoint, experiments indicate that they break down as the fractional bandwidth grows (see the examples that follow). This depends on the particular method, and the original array geometry. This may be due to accumulated interpolation error, but the precise cause is not entirely clear. As we have noted, and show in our examples, fractional bandwidths of interest in aeroacoustics may easily exceed 100%. Thus, the spatial resampling methods should be applied with some caution in cases of very large fractional bandwidth.

3.1.3 Other work

Buckley and Griffiths [32] provide an alternative to CSM based on the wideband spatio-temporal correlation matrix.

Sivanand et al. [41, 42, 43] show that the CSM focusing can be achieved in the time domain, and treat the problem from a multichannel FIR filtering perspective. They also consider beamforming.

Valaee and Kabal [47] present an alternative formulation of focussing matrices for CSM using a two-sided transformation (TCT). The method is an attempt to reduce the bias associated with CSM.

3.1.4 Performance Analysis

Cramer-Rao bounds (CRBs) on wideband AOA estimation can be established using either a deterministic or random Gaussian source model, in additive Gaussian noise. The basic results were shown by Bangs [30]; see also Swingler [46]. The deterministic source case in (possibly colored) Gaussian noise is described in Kay [35]. Performance analysis of spatial resampling methods is considered by Friedlander and Weiss, who also provide CRBs, as well as a description of maximum-likehood wideband AOA estimation [34].

These CRBs typically require known source statistics, and apply to unbiased estimates, whereas prior spectrum knowledge is typically not available, and the above wideband methods may result in biased estimates. Nevertheless, the CRB provides a valuable fundamental performance bound.

3.1.5 Wideband Beamforming

Basic extensions of narrow band beamforming methods are reviewed in Van Trees [48, chpt. 6], including delay-sum and wideband minimum variance distortionless response (MVDR) techniques. The CSM techniques also extend to wideband beamforming, e.g., see Yang and Kaveh [50].

3.1.6 Experiments

Example(s) and comparisons [39, 40].

3.1.7 Acknowledgements

Tien Pham.

3.2 Localization and tracking

Motivate issues in [17]: Array of arrays, large baselines, distributed signal processing versus communication bandwidth, signal coherence at widely separated sensors is not covered by small-scale models discussed in Section 2.

Physical models do not apply to long baselines, so we have little theoretical guidance about how much signal coherence to expect at widely spaced sensors. Our approach in [17]:

- Model sensor measurements as wideband Gaussian random processes with frequency-dependent coherence
- Consider zero-mean (strong scattering case), since plane waves are useless for time-delay estimation (TDE), and also because long baseline between sensors implies large distance to target, and large propagation distance tends toward strong scattering.

Show examples of coherence at widely spaced sensors

Communication versus distributed signal processing hierarchy:

1. Joint processing of all sensor data at a central node (maximum comm. BW, optimum performance)
2. Pass bearings from nodes, plus data from one sensor to enable TDE between pairs of sensors at central node
3. Pass bearings from nodes, triangulate the bearings at central node

Summarize conclusions: CRB says that bearings plus TDE with sensor pairs is nearly optimal, with significant savings in communication bandwidth, and significant improvement in localization accuracy compared with bearings-only triangulation. However, are the CRBs achievable? We study TDE with coherence losses caused by scattering. Need threshold coherence for a given SNR, fractional BW, and time-BW product. Implies for sources with sum-of-harmonics signature, need large time-BW product, but this is limited by source motion. Bring in Doppler ... Also discuss accounting for propagation time in the triangulation (refer to Kaplan?).

Conclusions: Need large SNR and time-BW product to achieve TDE CRBs, so in many cases, triangulation of bearings is optimum.

Show examples: TDE success with synthetic, wideband, non-moving source. TDE failure with moving ground vehicle. Cite standard references on triangulation of bearings ...

Ways to deal with moving sources:

- Our moving beamformer in [52], based on Gershman work.
- K. Bell's penalized ML for tracking bearings ...
- Paper on tracking in MSS '02 by Dave Hillis et. al. ... data association and other issues
- Kalman filter tracker (Bell, Kaplan, Hillis, others)
- Data association problem is worsened by aspect angle and Doppler. However, iterative processing may allow aspect angle and Doppler to be estimated and used to *improve* the data association.

3.3 Detection and classification

Specialize model to the energy of signals ...

Summarize probability of detection, from Keith's papers, e.g., [3] and [4].

Classification:

- Inherently difficult, because some vehicles have similar signatures
- Made more difficult by scattering during propagation, dependence of signatures on aspect-angle and source dynamics (change in velocity, Doppler)
- Show example from [51] with impact of scattering on harmonic amplitude signatures.
- Perhaps new classification results (probably won't be available).
- Open issues, such as whether knowledge of aspect angle (from tracker) can improve classification accuracy?

4 Concluding Remarks

Fill in ... Mention Doppler estimation and other continuing work.

References

[1] N. Srour and J. Robertson, "Remote netted acoustic detection system," Army Research Laboratory Technical Report, ARL-TR-706, May 1995.

[2] Paper in SPIE 2002 by Prado using small-aperture array ...

[3] D.K. Wilson, B.M. Sadler, T. Pham, "Simulation of detection and beamforming with acoustical ground sensors," *Proc. SPIE 2002 AeroSense Symp.*, Orlando, FL, April 1-5, 2002.

[4] D.K. Wilson, J.T. Kalb, N. Srour, T. Pham, B.M. Sadler, "Sensor algorithm interface and performance simulations in an acoustical battlefield decision aid," ARL Technical Report, **** Number??, 2002?**. (I don't have the final version of this report.)

[5] D.K. Wilson, "Performance bounds for acoustic direction-of-arrival arrays operating in atmospheric turbulence," *J. Acoust. Soc. Am.*, vol. 103, no. 3, pp. 1306-1319, March 1998.

[6] D.K. Wilson, "Atmospheric effects on acoustic arrays: a broad perspective from models," *1999 Meeting of the IRIS Specialty Group on Battlefield Acoustics and Seismics*, pp. 39–51, Laurel, MD, September 13-15, 1999.

[7] S.L Collier and D.K. Wilson, "Performance bounds for passive arrays operating in a turbulent medium: Plane-wave analysis," *J. Acoust. Soc. Am.*, Vol. 113, No. 5, pp. 2704–2718, May 2003.

[8] S.L Collier and D.K. Wilson, "Performance bounds for passive sensor arrays operating in a turbulent medium II: Spherical-wave analysis," in review at *J. Acoust. Soc. Am.*.

[9] D.E. Norris, D.K. Wilson, D.W. Thomson, "Correlations between acoustic travel-time fluctuations and turbulence in the atmospheric surface layer," *Acta Acustica*, vol. 87, pp. 677–684, 2001.

[10] D.K. Wilson, "A turbulence spectral model for sound propagation in the atmosphere that incorporates shear and buoyancy forcings", *J. Acoust. Soc. Am.*, **108** (5), Pt. 1, pp. 2021–2038, Nov. 2000.

[11] D.K. Wilson, C.R. Tate, D.C. Swanson, K.M. Reichard, "Acoustic scintillations and angle-of-arrival fluctuations observed outdoors with a large planar vertical microphone array," *Acoustics Research Letters Online*, vol. 106, no. 2, L24–L29, Aug. 1999. **** Need this? ****

[12] D.K. Wilson, G.L. Szeto, B.M. Sadler, R. Adams, N. Srour, "Propagation and array performance modeling for acoustic tracking of cruise missiles," *Proc. 1999 Meeting of the IRIS Specialty Group on Acoustic and Seismic Sensing*, ERIM International, Laurel, MD, 1999. **** Need this? ****

[13] S.M. Kay, V. Nagesha, J. Salisbury, "Broad-band detection based on two-dimensional mixed autoregressive models," *IEEE Trans. on Signal Processing*, vol. 41, no. 7, pp. 2413–2428, July 1993.

[14] M. Agrawal and S. Prasad, "DOA estimation of wideband sources using a harmonic source model and uniform linear array," *IEEE Trans. on Signal Processing*, vol. 47, no. 3, pp. 619–629, March 1999.

[15] M. Feder, "Parameter estimation and extraction of helicopter signals observed with a wide-band interference," *IEEE Trans. on Signal Processing*, vol. 41, no. 1, pp. 232–244, Jan. 1993.

[16] M. Zeytinoglu and K.M. Wong, "Detection of harmonic sets," *IEEE Trans. on Signal Processing*, vol. 43, no. 11, pp. 2618–2630, Nov. 1995.

[17] R.J. Kozick and B.M. Sadler, "Source Localization with Distributed Sensor Arrays and Partial Spatial Coherence," to appear in *IEEE Trans. on Signal Processing*, 2003.

[18] H.E. Bass, R. Raspet, and J.O. Messer, "Experimental determination of wind speed and direction using a three microphone array," *J. Acoust. Soc. Am.*, Vol. 97, pp. 695–696, 1995.

[19] P. Stoica, M. Agrawal, P. Ahgren, "Array processing for signals with non-zero means in colored noise fields," in review for *Digital Signal Processing: A Review Journal*, July 2003.

[20] D.I. Havelock, M.R. Stinson, G.A. Daigle, "Measurements of the two-frequency mutual coherence function for sound propagation through a turbulent atmosphere," *J. Acoust. Soc. Am.*, **104** (1), pp. 91–99, July 1998.

[21] A. Paulraj and T. Kailath, "Direction of arrival estimation by eigenstructure methods with imperfect spatial coherence of wavefronts," *J. Acoust. Soc. Am.*, vol. 83, pp. 1034-1040, March 1988.

[22] B.-G. Song and J.A. Ritcey, "Angle of arrival estimation of plane waves propagating in random media," *J. Acoust. Soc. Am.*, vol. 99, no. 3, pp. 1370-1379, March 1996.

[23] A.B. Gershman, C.F. Mecklenbrauker, J.F. Bohme, "Matrix fitting approach to direction of arrival estimation with imperfect spatial coherence," *IEEE Trans. on Signal Proc.*, vol. 45, no. 7, pp. 1894-1899, July 1997.

[24] O. Besson, F. Vincent, P. Stoica, and A.B. Gershman, "Approximate maximum likelihood estimators for array processing in multiplicative noise environments," *IEEE Trans. on Signal Processing*, vol. 48, no. 9, pp. 2506 -2518, Sept. 2000.

[25] J. Ringelstein, A.B. Gershman, and J.F. Bohme, "Direction finding in random inhomogeneous media in the presence of multiplicative noise," *IEEE Signal Processing Letters*, vol. 7, no. 10, pp. 269–272, Oct. 2000.

[26] P. Stoica, O. Besson, A.B. Gershman, "Direction-of-arrival estimation of an amplitude-distorted wavefront," *IEEE Trans. on Signal Processing*, vol. 49, no. 2, pp. 269–276, Feb. 2001.

[27] O. Besson, P. Stoica, A.B. Gershman, "Simple and accurate direction of arrival estimator in the case of imperfect spatial coherence," *IEEE Trans. on Signal Processing*, vol. 49, no. 4, pp. 730–737, April 2001.

[28] M. Ghogho, O. Besson, and A. Swami, "Estimation of directions of arrival of multiple scattered sources," *IEEE Trans. on Signal Processing*, vol. 49, no. 11, pp. 2467–2480, Nov. 2001.

[29] G. Fuks, J. Goldberg, H. Messer, "Bearing estimation in a Ricean channel–Part I: Inherent accuracy limitations," *IEEE Trans. on Signal Processing*, vol. 49, no. 5, pp. 925–937, May 2001.

[30] W. J. Bangs, "Array processing with generalized beamformers," PhD Dissertation, Yale University, 1972.

[31] J. F. Boehme, "Array processing," chapter 1 in *Advances in Spectrum Analysis and Array Processing, Vol. 2,* S. Haykin, ed. (Prentice-Hall, 1991).

[32] K. M. Buckley and L. J. Griffiths, "Broad-band signal-subspace spatial-spectrum (BASS-ALE) estimation," *IEEE Trans. ASSP,* Vol. 36, No. 7, pp. 953–964, July 1988.

[33] M. A. Doron, E. Doron, and A. J. Weiss, "Coherent wide-band processing for arbitrary array geometry," *IEEE Trans. SP,* Vol. 41, No. 1, pp. 414–417, January 1993.

[34] B. Friedlander, A. J. Weiss, "Direction finding for wide-band signals using an interpolated array," *IEEE Trans. SP,* Vol. 41, No. 4, pp. 1618–1634, April 1993.

[35] S. M. Kay, *Fundamentals of Statistical Signal Processing, Estimation Theory* (Prentice-Hall, 1993).

[36] J. Krolik and D. Swingler, "Focused wide-band array processing by spatial resampling," *IEEE Trans. ASSP,* Vol. 38, No. 2, pp. 356–360, February 1990.

[37] J. Krolik, "Focused wide-band array processing for spatial spectral estimation," chapter 6 in *Advances in Spectrum Analysis and Array Processing, Vol. 2,* S. Haykin, ed. (Prentice-Hall, 1991).

[38] N. Owsley, "Sonar array processing," in *Array Signal Processing,* S. Haykin ed. (Prentice-Hall, 1984).

[39] T. Pham, B. M. Sadler, "Adaptive wideband aeroacoustic array processing," *Proc. 8th IEEE Signal Processing Workshop on Statistical Signal and Array Processing,* pp. 295–298, June 1996.

[40] T. Pham, B. M. Sadler, "Focused wideband array processing algorithms for high-resolution direction finding," *Proc. MSS meeting,* Sept. 1998.

[41] S. Sivanand, J. Yang, and M. Kaveh, "Focusing filters for wide-band direction finding," *IEEE Trans. SP,* Vol. 39, No. 2, pp. 437–445, February 1991.

[42] S. Sivanand and M. Kaveh, "Multichannel filtering for wide-band direction finding," *IEEE Trans. SP,* Vol. 39, No. 9, pp. 2128–2132, September 1991.

[43] S. Sivanand, "On focusing preprocessor for broadband beamforming," *Sixth SP Workshop on Stat. Sig. and Array Proc.,* pp. 350–353, Victoria, BC, Canada, October 1992.

[44] G. Su, M. Morf "Signal subspace approach for multiple wideband emitter location," *IEEE Trans. ASSP,* Vol. 31, no. 6, pp. 1502–1522, December 1983.

[45] D. N. Swingler and J. Krolik, "Source location bias in the coherently focused high-resolution broad-band beamformer," *IEEE Trans. ASSP,* Vol. 37, No. 1, pp. 143–145, January 1989.

[46] D. N. Swingler, "An approximate expression for the Cramer-Rao bound on DOA estimates of closely spaced sources in broadband line-array beamforming," *IEEE Trans. SP,* Vol. 42, No. 6, pp. 1540–1543, June 1994.

[47] S. Valaee and P. Kabal, "Wideband array processing using a two-sided correlation transformation," *IEEE Trans. SP,* Vol. 43, No. 1, pp. 160–172, January 1995.

[48] H. L. Van Trees, *Optimum Array Processing* (Wiley, 2002).

[49] H. Wang and M. Kaveh, "Coherent signal-subspace processing for the detection and estimation of angles of arrival of multiple wide-band sources," *IEEE Trans. ASSP,* Vol. ASSP-33, No. 4, pp. 823–831, August 1985.

[50] J. Yang and M. Kaveh, "Coherent signal-subspace transformation beamformer," *IEE Proc.,* Vol. 137, Pt. F, No. 4, pp. 267–275, August 1990.

[51] R.J. Kozick and B.M. Sadler, "Information Sharing Between Localization, Tracking, and Identification Algorithms," *Proc. 2002 Meeting of the MSS Specialty Group on Battlefield Acoustics and Seismics*, Laurel, MD, Sept. 24–27, 2002.

[52] R.J. Kozick and B.M. Sadler, "Tracking Moving Acoustic Sources with a Network of Sensors," Army Research Laboratory Technical Report ARL-TR-2750, October 2002.